PREDICTION OF INDIVIDUAL VARIATION OF SECOND-PARTY PUNISHMENT FROM RESTING-STATE FUNCTIONAL CONNECTIVITY

by

Fengying Ding

A Thesis
Submitted to the
Graduate Faculty
of
George Mason University
in Partial Fulfillment of
The Requirements for the Degree
of
Master of Science
Bioinformatics and Computational Biology

Committee:

_____	Dr. Frank Krueger, Thesis Director
_____	Dr. William Kennedy, Committee Member
_____	Dr. Nadine Kabbani, Committee Member
_____	Dr. Iosif Vaisman, Director, School of Systems Biology
_____	Dr. Donna Fox, Associate Dean, Office of Student Affairs & Special Programs, College of Science
_____	Dr. Peggy Agouris, Dean, College of Science
Date: _____	Spring Semester 2019 George Mason University Fairfax, VA

Prediction of Individual Variation of Second-party Punishment from Resting-state Functional Connectivity

A Thesis submitted in partial fulfillment of the requirements for the degree of Master of Science at George Mason University

by

Fengying Ding
Bachelor of Engineering
Beijing Institute of Technology (Zhuhai), 2015

Director: Frank Krueger, Associate Professor
School of Systems Biology

Spring Semester 2019
George Mason University
Fairfax, VA

DEDICATION

This is dedicated to my parents, sister, brother, and friends.

ACKNOWLEDGEMENTS

I would like to thank the many friends, relatives, and supporters who have made this happen. Dr. Krueger was of invaluable help. Thanks go out to the Fenwick Library for providing a clean, quiet, and well-equipped repository in which to work. The data for this this thesis was collected at the University of Mannheim/ University of Heidelberg in Germany. I am responsible for analyzing data and writing the thesis.

TABLE OF CONTENTS

LIST OF TABLES

Table Page

LIST OF FIGURES

Figure Page

LIST OF ABBREVIATIONS

amygdala ..... amyg
anterior insula ..... AI
blood-oxygen-level-dependent ..... BOLD
central executive network ..... CEN
cingulo-opercular network ..... CON
default-mode network ..... DMN
dictator game ..... DG
dorsal anterior cingulate cortex ..... dACC
dorsolateral prefrontal cortex ..... dlPFC
dorsomedial prefrontal cortex ..... dmPFC
frontoparietal network ..... FPN
Functional Connectivity toolbox ..... CONN
Functional Magnetic Resonance Imaging ..... fMRI
independent component analysis ..... ICA
leave-one-subject-out cross-validation ..... LOSOCV
medial prefrontal cortex ..... mPFC
monetary units ..... MUs
multivariate prediction analysis ..... MVPA
occipital network ..... OccN
posterior cingulate cortex ..... PCC
posterior parietal cortex ..... PPC
regions of interest ..... ROI
resting-state functional connectivity ..... RSFC
resting-state functional magnetic resonance imaging ..... RS-fMRI
salience network ..... SAN
second-party punishment ..... SPP
sensorimotor network ..... SMN
standardized mean squared error ..... SMSE
support vector machine ..... SVM
temporo-parietal junction ..... TPJ
third-party punishment ..... TPP
ultimatum game ..... UG
ventromedial prefrontal cortex ..... vmPFC

ABSTRACT

PREDICTION OF INDIVIDUAL VARIATION OF SECOND-PARTY PUNISHMENT FROM RESTING-STATE FUNCTIONAL CONNECTIVITY

Fengying Ding, M.S.

George Mason University, 2019

Thesis Director: Dr. Frank Krueger

Social norms and associated altruistic behaviors are significant for human society. Humans are willing to punish the violators of social norms at their personal costs (i.e., costly second-party punishment, SPP), which can be measured with socio-economic exchange games. From the view of psychology, SPP is driven by blame, integrating the harm of victim and intent of offender. From the perspective of neural network, SPP behavior is associated with salience network, default-mode network and central-executive network (CEN). Although SPP is associated with large-scale brain networks regulating social-cognitive processes measured with task-based functional magnetic resonance imaging (fMRI), the prediction of individual variation of SPP behavior based on resting-state functional connectivity (RSFC) measured with task-free fMRI has not yet been established. The aim of this master thesis was to predict individual differences in SPP—measured via a two-person economic exchange game— based on RSFC combining task-free fMRI with a multivariate prediction analysis (MVPA). First, we showed on the behavioral level that SPP increased with the

degree of unfair offers in the SPP game. Second, we demonstrated on the neural level, that variation in average SPP behavior was predicted through RSFC within the central-executive network confirming that CEN is the driving network for the determination of SPP behavior. In conclusion, our study provides a comprehensive picture regarding SPP behavior for maintaining human social norms.

1. THERERICAL BACKGROUND

1.1 Second-Party Punishment as a Form of Costly Punishment

Human society is unique for the compliance of social norms and the associated altruistic behavior (Baumgartner, Götte, Gügler, & Fehr, 2012; Buckholtz & Marois, 2012). To maintain a stable human society, humans are willing to punish the violators of social norms at their personal costs (i.e., costly punishment) (Henrich et al., 2006; Rockenbach & Milinski, 2006). Costly punishment is costly to the punisher, but it is more costly to the punished (Hauert, Traulsen, Brandt, Nowak, & Sigmund, 2007; Kuwabara & Yu, 2017). It is this kind of punishment that discourage cheaters, therefore, enforcing cooperation among people in human society (Rockenbach & Milinski, 2006).

Two types of costly punishment exist: second-party punishment (SPP) and third-party punishment (TPP). Not only victims (i.e., SPP) but also the witnesses who are not affected by the violation (i.e., TPP) are willing to punish the violators (i.e., offenders) (Bendor & Swistak, 2001; Sober, Wilson, & Wilson, 1999). Unfair treatment and negative emotions (such as aversion and anger) lead to SPP (Pillutla & Murnighan, 1996). Although third parties are not affected psychologically by the unfair treatment to second parties, they are willing to punish the violators when they witness the norm violation (Fehr & Fischbacher, 2004b; Henrich, 2006).

1.2 Economic Games as Instruments to Measure Second-Party Punishment

Economic exchange games can be used to measure costly punishment behavior, revealing the essential role of SPP in the compliance of social norms (Henrich et al., 2006; Leibbrandt & López-Pérez, 2012). The SPP game is extension of the ultimatum game (UG) (McAuliffe, 2017; Strobel et al., 2011). In the UG, proposers send an offer (i.e., a split of an endowment of money) to receivers who can either accept or decline the offer (Gospic et al., 2011). In the SPP game, both proposers and responders are endowed with a certain amount of money (Henrich et al., 2006; Leibbrandt & López-Pérez, 2012). Then, proposers are given extra money to share with receivers. An offer of 30% of the given MUs is considered as fair (Fehr & Fischbacher, 2003; Wallace, Cesarini, Lichtenstein, & Johannesson, 2007). If proposers share an unfair amount of money with responders, they can use their money to punish the proposers (**Figure 1**) (Henrich et al., 2006; Leibbrandt & López-Pérez, 2012). The amount of punishment depends on the fairness of the offer (i.e., fair vs. unfair outcome) to the receivers and the intention of the proposers behind the offer (i.e., good or bad intention) (Krueger & Hoffman, 2016).

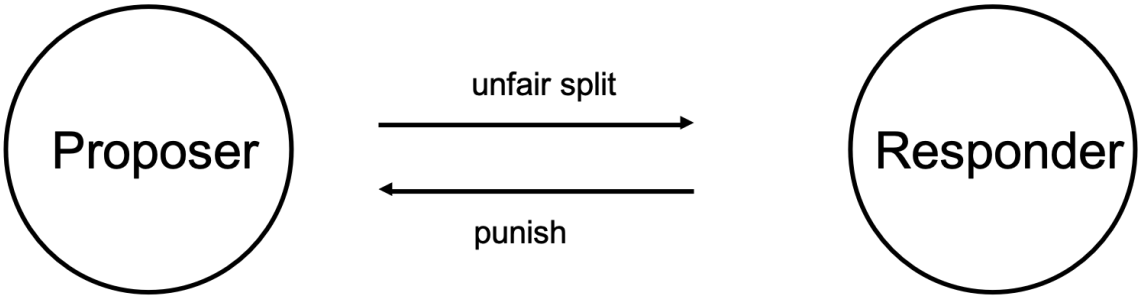

Figure 1. Second-Party Punishment Game.

Proposer and responders interact in the second-party punishment game by using an endowment of money. Proposer make an offer on how to split the money and depending on the fairness of the offer responders can punish the proposer using their money.

1.3 Neuropsychological Framework of Second-Party Punishment

Punishment is determined by the blame that is based on intention (i.e., good vs. bad) of the proposer and the severity of harm (i.e., fair vs. unfair outcome) inflicted on the responder (Figure 2A) (Krueger & Hoffman, 2016) (**Figure 2B**).

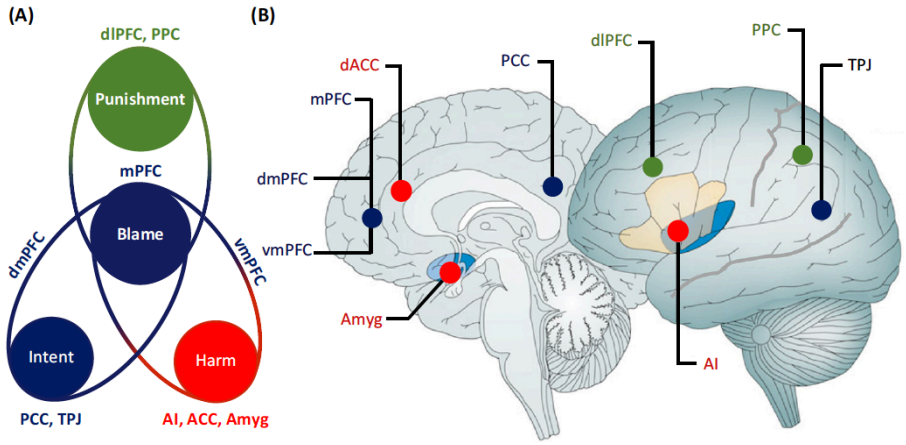

Figure 2. Neuropsychological Framework of Second-Party Punishment.

(A) Psychological Framework. Second-party punishment is driven by blame, which is determined based on the intent behind the social norm violation (i.e., proposer's good or bad the offer) and the harm (i.e., fair vs. unfair offer) inflicted on the receiver. **(B) Large-Scale Networks.** Three large-scale brain networks —salience network (red), default mode net-work (blue), and central executive network (green) — are involved in SPP (Figure taken from Krueger & Hoffman, 2016).

SPP behavior is associated with the interaction of three large-scale brain networks (Krueger & Hoffman, 2016): salience network (SAN), default-mode network (DMN) and central-executive network (CEN) (**Figure 2B**) (Bressler & Menon, 2010; Buckholtz & Marois, 2012; Krueger & Hoffman, 2016).

The SAN— associated with *aversive self-related emotional experiences* that guide behavior— includes the dorsal anterior cingulate cortex (dACC) (detection of social norm violation), the anterior insula (AI) (generation of an aversive experience), and the amygdala (Amyg) (provides an emotional signal coding for the severity of harm, i.e., unfairness of the offer) (Bressler & Menon, 2010; Krueger & Hoffman, 2016).

The DMN —associated with social cognition, mentalizing, and theory of mind— is anchored in medial prefrontal cortex (mPFC) (Premack & Woodruff, 1978). This network integrated harm [via the ventromedial prefrontal cortex (vmPFC) connected to SAN] and the intent of the proposer [via the dorsomedial prefrontal cortex (dmPFC), including posterior cingulate cortex (PCC) for self-referential and temporo-parietal junction (TPJ) for intentions, beliefs or desires in others] into assessment of blame through the medial prefrontal cortex (mPFC).

The CEN —associated with higher-order cognition and decision making— converts the blame signal from the DMN into an actual decision, posterior parietal cortex (PPC) constructing a scale of punishment for dorsolateral prefrontal cortex (dlPFC) to select punishment that fits the norm violation (Bellucci et al., 2017; Bressler & Menon,

2010; Buckholtz et al., 2008, 2015; Krueger & Hoffman, 2016; Krueger, Hoffman, Walter, & Grafman, 2014).

1.4 Resting-State Functional Magnetic Resonance Imaging

Functional magnetic resonance imaging (fMRI) is a technique widely used to study brain functions (Logothetis, Pauls, Augath, Trinath, & Oeltermann, 2001; Voos & Pelphrey, 2013). Neural activity can be reflected by the oxygen in the blood. Thus, localizing changes in brain blood flow and blood oxygenation, the blood-oxygen-level-dependent (BOLD) signal reflects changes in deoxyhemoglobin (Arthurs & Boniface, 2002; Hillman, 2014; Keller et al., 2013). Contrary to oxygenated hemoglobin, deoxygenated hemoglobin is paramagnetic and has the ability to distort surrounding magnetic field (Pauling & Coryell, 1936). Due to the difference of magnetic susceptibility between oxygenated hemoglobin and deoxygenated hemoglobin, the BOLD signal changes relying on the hemodynamic response in a brain region.

Brain functions can be quantified via *task-based fMRI* studies that uses relative changes from baseline in BOLD signal during a task to infer the activation of certain areas(Lee, Smyser, & Shimony, 2013). Task-based fMRI was used to study costly punishment (SPP and TPP): to reveal the neural underpinnings regarding third-party decision-making related to criminal responsibility and punishment (Buckholtz et al., 2008); to study the social norm enforcement by unaffected third parties (Zhong, Chark, Hsu, & Chew, 2016); to investigate the neural signatures regarding the modulations of responsibility on altruistic punishment (C. Feng et al., 2016); to study self-related and

fairness-related neural mechanism by UG (Corradi-Dell'Acqua, Civai, Rumiati, & Fink, 2013); to investigate the neural basics of economic decision-making on UG (Sanfey, Rilling, Aronson, Nystrom, & Cohen, 2003), to reveal the abnormal brain responses to social fairness in depression by fMRI study in UG (Gradin et al., 2015).

Resting-state functional magnetic resonance imaging (RS-fMRI) is a powerful tool to examine task-independent brain activity, making an assessment for brain regions which may not be involved in the task (Khadka et al., 2013; Oathes, Patenaude, Schatzberg, & Etkin, 2015). This method allows intrinsic functional activity and connectivity of brain circuits— consistently, and reliably, yielding large sample sizes and good compliance in adolescents, enabling developmental studies using a single imaging dataset— to be examined across various brain networks and regions (Oathes et al., 2015). RS-fMRI can be acquired quickly (5-10 mins). During RS-fMRI experiment, individuals lie in the scanner, close their eyes, thinking nothing without falling asleep (M. P. van den Heuvel & Hulshoff Pol, 2010).

Coherent low-frequency (0.01-0.1 Hz) BOLD fluctuations in distant grey matter regions represent RS-fMRI, integrating the brain function (Biswal, Zerrin Yetkin, Haughton, & Hyde, 1995; Finn et al., 2015). Using different subjects, different methods, and different MR acquisition techniques (such as vendor, field strengths) and different analysis techniques (such as seed methods, independent component analysis, clustering), researches get consistently results for functional related RS brain networks (Beckmann, DeLuca, Devlin, & Smith, 2005; Biswal, Yetkin, Haughton, & Hyde, 1995; Damoiseaux

et al., 2006; De Luca, Beckmann, De Stefano, Matthews, & Smith, 2006; M. van den Heuvel, Mandl, & Pol, 2008; Salvador et al., 2005).

RS-fMRI can be measure by different methods: model-dependent methods (i.e., seed method) and model-free methods (e.g., independent component analysis; ICA) (D. Cordes et al., 2000; Fransson, 2005; (Beckmann, DeLuca, Devlin, & Smith, 2005; Calhoun, Adali, Pearlson, & Pekar, 2001). Through those methods, several functionally linked sub-networks have been identified (Beckmann, DeLuca, Devlin, & Smith, 2005; Damoiseaux et al., 2006), including SAN, DMN, and CEN (**Figure 3**). They are also stable and consistent networks activated by a broad spectrum of task-based studies (Kelly, Biswal, Craddock, Castellanos, & Milham, 2012). Recent research has indicated that RSFC reflects an individual's neural fingerprint regarding personality traits, social preferences, and prosocial behaviors (Bellucci, Hahn, Deshpande, & Krueger, 2019; Nash, Gianotti, & Knoch, 2015; Nash et al., 2015); However, RSFC has not been applied for identifying core networks of costly punishment.

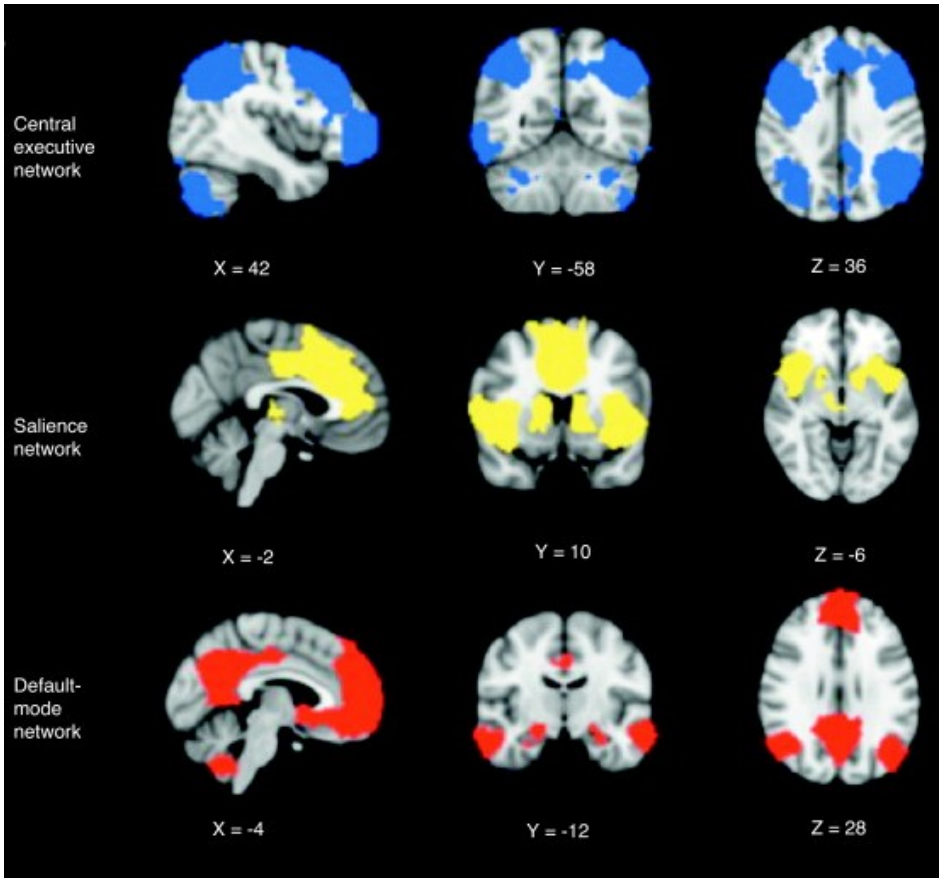

Figure 3. Resting-State Brain Networks.

Several resting-state brain networks have been identified—central-executive network (blue), salience network (yellow). and default- mode network (red), which are stable across time and strikingly like the networks activated by a broad spectrum of task-based neuroimaging studies (Figure taken form Menon, 2011).

1.5 Machine Learning and Prediction-Analytics Framework

Machine learning by multivariate prediction analysis (MVPA) (i.e., prediction-analytics framework) is used to train training set to build a model regarding costly punishment measured by RSFC (Craddock, Holtzheimer, Hu, & Mayberg, 2009; Gordon, Devaney, Bean, & Vaidya, 2015; Kelly et al., 2012). The predictive model is implemented in a

separated testing set to predict costly punishment. Model is estimated through comparing the result of predictions to true costly punishment. This model is able to use feature selection to extract useful information and reduce the input variables to the most relevant variables. MVPA has been used to fMRI and RSFC data (Wang, Han, He, Liu, & Bi, 2012; Wu, Li, Yuan, & Tian, 2016). The significance of an entire RSFC pattern can be evaluated by MVPA (Parisi et al., 2014; Richiardi, Achard, Bunke, & Ville, 2013).

Previous studies have shown that MVPA has been used to make predictions (D'Amico et al., 1995; de Blacam et al., 2012; Demers et al., 1992). It can identify RSFC neuromarkers for disorders such as Alzheimer's disease in non-demented at risk patients (Teipel et al., 2007), schizophrenia (Radua et al., 2010; H. Shen, Wang, Liu, & Hu, 2010), and autism (Anderson et al., 2011) but also for age (Dosenbach et al., 2010), personality traits (Hahn, Buttaccio, Hahn, & Lee, 2015), and prosocial behavior (trust). However, it has not been used to predict individual variation in SPP behavior.

1.6 Study Aims and Hypotheses

Although RSFC is an appealing substitute for the task-based fMRI approach to characterize neurodiversity (Bellucci, Hahn, Deshpande, & Krueger, 2018; DE Gabrieli, Ghosh, & Whitfield-Gabrieli, 2015), no study so far has used RSFC to predict individual variations in SPP behavior. The goal of this study was to combine a SPP game with RS-fMRI and a prediction framework using MVPA to investigate whether individual differences in SPP can be predicted based on RSFC. First, we hypothesized SPP behavior increases with more unfair offers and second parties punish more than third parties, because punisment is driven

by blame, integrating harm of second parties and intent of third parties. Second parties foucus more on harm while third parties focus more on intent. Further, we hypothesized that individual variations in average SPP behavior can be predicted by RSFC in CEN, because it is the key network in determining the punishment decision (Bellucci et al., 2017; Bressler & Menon, 2010; Buckholtz et al., 2008, 2015; Krueger & Hoffman, 2016; Krueger, Hoffman, Walter, & Grafman, 2014).

2. MATERIAL AND METHODS

2.1 Participants

In this study, 52 healthy participants (28 females, 24 males, age in years: *Mean* = 23.52, *Standard Deviation* = 3.17) recruited from the University of Mannheim or the University of Heidelberg in Germany took part in this study. The study followed the ethical guidelines and principles of the Declaration of Helsinki; it was approved by the local ethics committee. All participants gained 35€ for their participation and were informed that the earned monetary units (MUs) during the economic exchange game will be converted into real money (maximum of 10€) and paid on top at the end of the experiment.

2.2 Experimental Game Paradigms

Participants played three different one-shot exchange games: dictator game (DG), SPP game, and TPP game (Strobel et al., 2011). In the DG (i.e., control game), participants played the role of proposers (i.e., dictators) who were given 12 MU to share with receivers who had to accept this offer. Next, participants played either the SPP game and TPP game in a counter balanced manner.

In the SPP game, both proposers and receivers were endowed with 6 MUs and proposers were given extra 12 MUs to share with receivers (**Figure 4**). Participants played as responders and were asked to decide whether to punish the proposers based on seven randomly received offers ranging from fair to unfair (6:6; 7:5; 8:4; 9:3; 10:2; 11:1; 12:0). For a fair offer, when proposers give 6 MUs to receivers, they will usually not be punished

by receivers. However, for an unfair offer, for example, when proposers keep all the money (i.e., unfair offer: 12:0), receivers can use their 6 MUs to punish proposers. Each MU spent for punishment reduces the total amount of proposers by a factor of 3 MUs (Baumgartner et al., 2012). If receivers, for example, use their 6 MUs to punish, proposers' total amount of 18 MUs (6 MUs initial endowment plus 12 MUs kept) will be reduced by 18 MUs (3 x 6 MUs), which leaves both proposers and receivers with 0 MUs and the end of the economic exchange (Strobel et al., 2011).

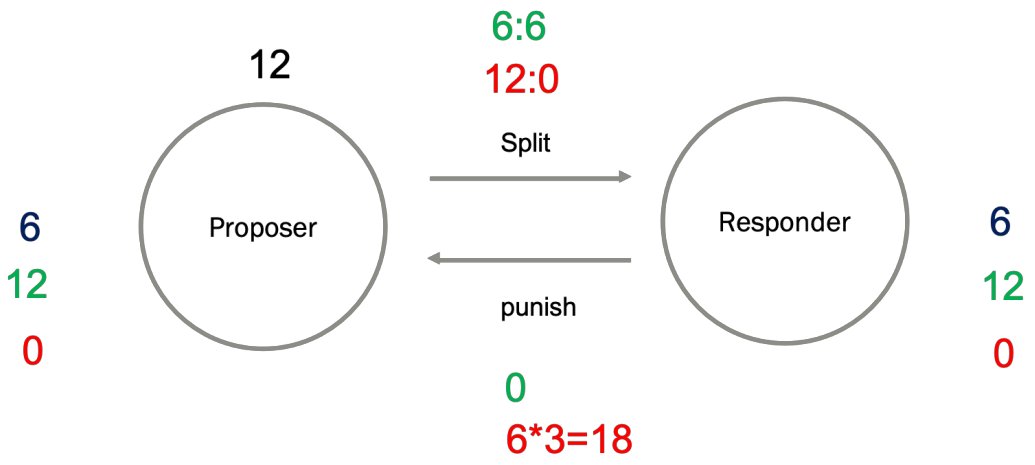

Figure 4. Description of Second-Party Punishment Game.

In the second-party punishment game, proposers and responders were endowed with 6 monetary units (MUs, black color) and proposers was given extra 12 MUs to share with responders (unfair offer, red; fair offer green), and responders had the chance to punish proposers; each MU spent for punishment reduces the total amount of proposers by a factor of 3 MUs.

The TPP game served as another control game: an observer (third-party) was added in comparison to the SPP game. In this game, proposers and observers (i.e., third-parties) were endowed with 6 MUs (**Figure 5**). Participants played as third parties and were asked to decide whether to punish the proposers based on seven randomly received offers ranging from fair to unfair (6:6; 7:5; 8:4; 9:3; 10:2; 11:1; 12:0). Proposers were asked to share their extra given 12 MUs to share with receivers. In this context, receivers have to accept the offers but the unaffected third-parties had the opportunity to punish the proposer at their own expenses. For a fair offer, when proposers give 6 MUs to receivers, third parties will usually not punish proposers. However, for an unfair offer, for example, when proposers keep all the money (i.e., unfair offer: 12:0), third parties can use their 6 MUs to punish proposers. Each MU spent for punishment reduces the total amount of proposers by a factor of 3 MUs (Baumgartner et al., 2012). If third parties, for example, use their 6 MUs to punish, proposers' total amount of 18 MUs (6 MUs initial endowment plus 12 MUs kept) will be reduced by 18 MUs (3 x 6 MUs), which leaves all of them (proposers, receivers and third parties) with 0 MUs and the end of the economic exchange (Strobel et al., 2011).

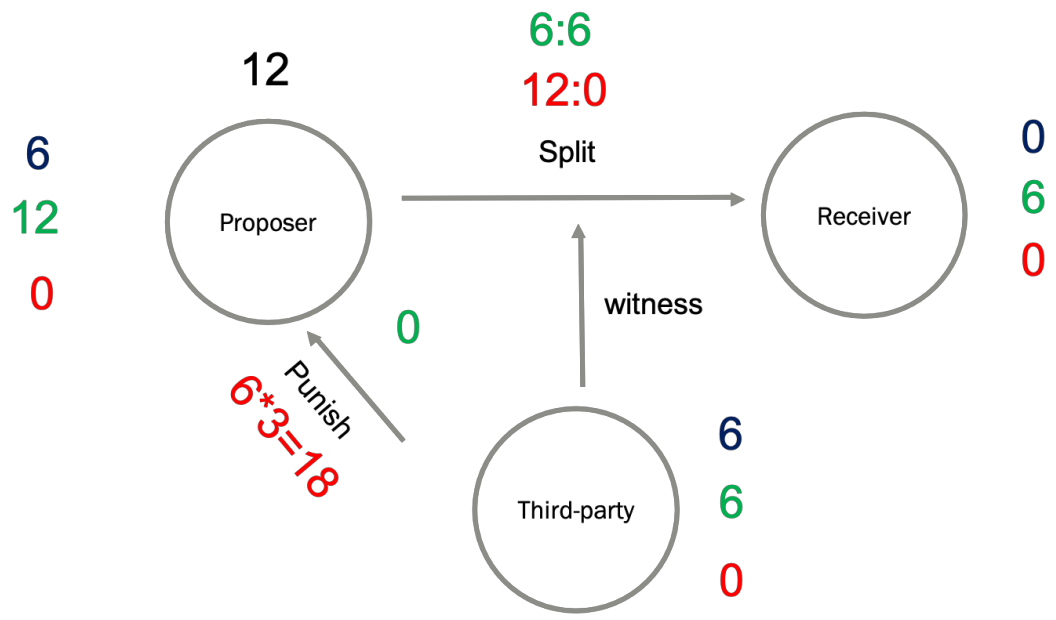

Figure 5. Description of Third-Party Punishment Game.

In the third-party punishment game, proposers and responders were endowed with 6 monetary units (MUs, black color). Proposers was given extra 12 Mus to share with receivers who can only accept the offer (unfair offer, red; fair offer, green). Third-party witnessed the offer and had the chance to punish proposers; each MU spent for punishment reduces the total amount of proposers by a factor of 3 MUs.

2.3 Procedure

The study consisted of two parts: first, participants were asked to complete the economic games and a demographic survey using the Qualtrics online platform (https://www.qualtrics.com) and second, participants completed a structural MRI and a RS-fMRI scan, each lasting about 10 minutes.

2.4 Analysis of Behavioral Data

The software package SPSS 24.0 (IBM Corp, 2016) was used to analyze the behavioral data. Alpha was set to $p < 0.05$ (two tailed) for all statistical analysis. First, the means and standard errors of mean were calculated for the average punishment and across all levels of offers (6:6, 7:5, 8:4, 9:3, 10:2, 11:1, 12:0). Second, a repeated measures 7 Offer (6:6, 7:5, 8:4, 9:3, 10:2, 11:1, 12:0) x 2 Type (SPP vs. TPP) analysis of variance (ANOVAS) on costly punishment behaviors was calculated with Offer and Type as within-subjects factors. Third, a one-way ANOVA on SPP behavior with Offer (6:6, 7:5, 8:4, 9:3, 10:2, 11:1, 12:0) as a within-subjects factor was performed to determine the slope of punishment from the most fair offer (i.e., 6:6) to the most unfair offer (i.e., 12:0). Finally, a paired-samples *t* test was computed to compare the average punishment behaviors between SPP and TPP.

2.5 Acquisition of MRI Data

A Siemens TRIO-3T MRI scanner (Siemens Medical Systems, Erlangen, Germany) with a 32-channel head coil were used to collect the neuroimaging data. First, to collect a high resolution anatomical scan of the entire brain for each participant, a T1-weighted 3D magnetization prepared rapid acquisition was utilized with gradient echo (MP-RAGE) sequence: time of repetition (TR), 2300 ms; TE, 3.03 ms; flip angle, 9°; number of slices, 192; field of view (FOV), 256 mm; matrix size, 256 x 256; voxel size, 1 x 1 x 1 mm was utilized. Second, to measure the BOLD signal for functional images a T2-weighted gradient EPI was measured with the following parameters: TR, 2000 ms; TE, 30ms; flip angle, 80°; thickness, 3mm; number of slices, 36; FOV, 192 mm; matrix size, 64 x 64 mm;

voxel size, 3 x 3 x 3 mm. The first five scans of the EPI were discarded to minimize T1 effects.

2.6 Analysis of Neuroimaging Data

MRI Data Preprocessing. The Statistical Parametric Mapping toolbox (SPM 12, Wellcome Trust Centre for Neuroimaging, London, UK; http://www.fil.ion.ucl.ac.uk/spm/software/spm12/) running on Matlab R2018a (Mathworks Inc., Natick, MA, USA) was used to preprocess the MRI data. The following preprocessing steps for the EPI time series were applied: For signal improvement, the first ten volumes of functional images were initially discarded, and the functional images were bias-corrected for field inhomogeneity. Spatial realignment was used to correct for head movement and slice time correction for acquisition delay. Participants' individual functional images were co-registered to their anatomical images and both anatomical images and functional images were spatially normalized to the MNI template (resample voxel size: $2 \times 2 \times 2$ mm^3). Finally, an isotropic Gaussian filter of 4 x 4 x 4 mm^3 with a full-width at half of maximum (FWHM) were used to smooth normalized images.

The ART toolbox (ART, https://www.nitrc. org/projects/artifact_detect/) was used to detect and reject artifacts in the time series of functional images based on the those criteria: (1) head displacement in x, y, or z-direction greater than 2 mm from the previous frames; (2) rotational displacement greater than 0.02 radians from the previous frame, and (3) global mean intensity in the functional images greater than 3 standard deviations compared with mean image intensity during the entire resting-state scanning. Finally, high-

frequency noise and linear drift artifacts were removed using the band-pass filter (0.01-0.1 Hz) (Bellucci et al., 2017).

Resting-State Functional Connectivity. The computation of RSFC was based on 142 regions of interest (ROIs; nodes) taken from the Dosenbach's atlas (Dosenbach et al., 2010) (**Figure 6**). Those ROIs (each 10-mm sphere) can be divided into five pre-defined RSFC networks (cingulo-opercular network (CON, also known as SAN), sensorimotor network (SMN), default-mode network (DMN), frontoparietal network (FPN, also known as CEN) and occipital network (OccN).

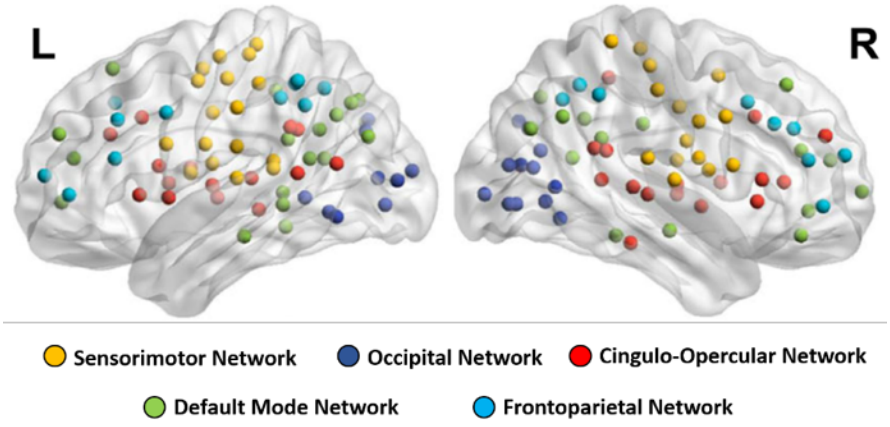

Figure 6. Resting-state Functional Connectivity Networks based on Dosenbach's Atlas.

Dosenbach's Atlas consisting of five resting-state functional connectivity networks shown in different colors: sensorimotor network (yellow), and occipital network (purple), cingulo-opercular network (red), default mode network (green), frontoparietal network (blue) (Adjusted from Bellucci et al., 2017).

The RSFC was based on a bivariate Pearson's correlation between the average BOLD signals of each ROI using the Functional Connectivity toolbox (CONN) (https://www. nitrc.org/projects/conn). Regressors of no interest were added in the first-level general linear model, including six head motion parameters (three translations and three rotations along x, y, and z- axes), outliers derived from the ART toolbox, white matter and cerebrospinal fluid signal, to remove potential sources of confounds. The Pearson's correlation co-efficient obtained for each ROI-to-ROI connection (edge) were converted to Fisher's z values to indicate the degree of ROI-to-ROI connectivity. As a result, an correlation matrix of 10,082 connections for each participant was created and used in the subsequent multivariate regression analyses.

Prediction-Analytics Framework. A support vector machine algorithm (SVM), using the sci-kit-learn toolbox (https://scikit-learn.org/stable/) in Python (https://www.python.org/), was employed to predict individual variations in SPP behavior based on RSFC. A total of 15 prediction models were employed: five intra-network specific models (CON-CON, SMN-SMN, FPN-FPN, DMN-DMN, OccN-OccN) and ten inter-network models (DMN-FPN, CON-FPN, OccN-SMN, DMN-OccN, CON-OccN, CON-DMN, FPN-OccN, FPN-SMN, DMN-SMN, CON-SMN).

A leave-one-subject-out cross-validation (LOSOCV) approach was applied for each prediction model. For each iteration, a training set was trained by the SVM algorithm —except one of the participants (testing set) was left out and was not trained by the

algorithm. A feature selection approach was applied for the training set due to the high-dimensionality of the features (ROI-to-ROI FCs coefficients, n=10,082), where only 5% of the strongest correlations between the features and the targets (i.e., SPP behavior) were kept as the most relevant features. Those features were trained by the algorithm and the features from the left-out subject was used to test the model performance. Iteration was repeated 52 times (i.e., number of participants). Hence, 52 models were generated, yielding each time a behavioral prediction for each participant.

To assess performance of a model's prediction, the standardized mean squared error (SMSE. i.e., the error of the algorithm's performance divided by the targets' variance) was computed. To assess the significance of the prediction, a permutation test of 1,000 permutations was utilized. In every permutation, each cross-validated model was run with randomly permuted targets, and the number of permutations with better performance (i.e., lower SMSE) than the one with the true targets was calculated (i.e., n_{perm}). The p-value was computed by dividing this number by the total number of permutations, i.e., $p = (1 + n_{perm})/(1 + 1{,}000)$ (Bellucci et al., 2018).

Network Ranking Procedure. After applying paired-samples t tests (i.e., comparing the distributions between the original and permutation-based prediction errors for each of the networks), a 15*15 p-value matrix was generated to compare the regression model performance between the 15 networks (i.e., five intra-networks and ten inter-between networks). A significant p-value indicated whether the prediction error for one network is significantly greater than that for another one. This p values indicates how significantly

one network predicts costly punishment behavior (i.e., target variable) compared to other networks. Hence, all p-values can be used to rank networks and the highest-ranking network is the best network to predict SPP behavior.

3. RESULTS

3.1 Behavioral Results for Second-Party Punishment Behavior

For each punishment type (TPP, SPP), the means and standard errors of mean for the average punishments across offers as well as for each offer are displayed in Figure 7. The ANOVA revealed significant main factor effects for Offer ($F(6,306)=4.71$, $p<0.035$) and Type ($F(1,51)=30.44$, $p<0.001$), but no significant Offer x Type interaction effect ($F(6,306)=0.65$, $p=0.648$). Punishment behavior increased linearly from the most fair offer (i.e., 6:6) to the most unfair offer (i.e., 12:0) ($F(1,51)=26.24$, $p<0.001$) and average SPP behavior was greater compared to TPP behavior ($t(51)=2.17$, $p<0.035$).

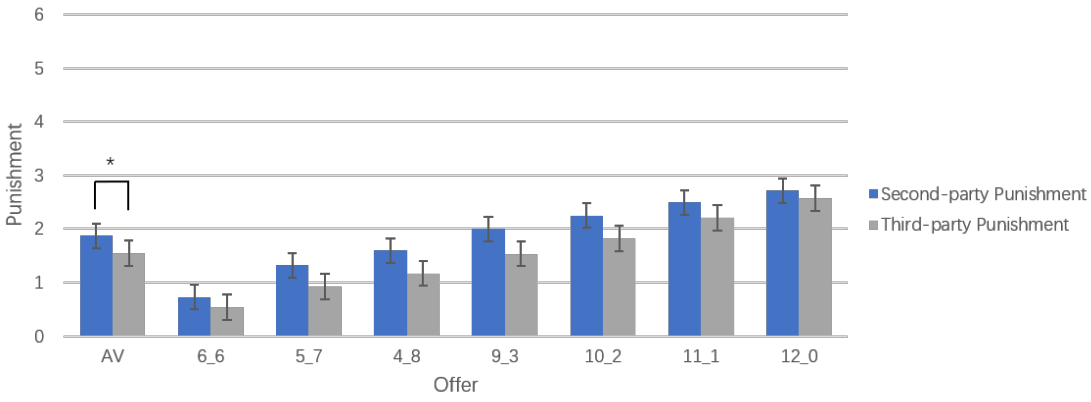

Figure 7. Behavioral Results for Costly Punishment Behavior.

Costly punishment behavior (mean ± standard error of mean) increased linearly from 6:6 (fair) over 7:5, 8:4, 9:3 10:2, 11:1 to 12:0 (most unfair) offer. The average of second-party punishment was higher than the average of third-party punishment (*p<0.05).

3.2 Neuroimaging Results for Second-Party Punishment Behavior

Multivariate Prediction Analyses. A SVM machine learning algorithm was implemented to predict participants' SPP behavior based on RSFC of 15 networks (i.e., five inter-networks and ten inter-networks) (Dosenbach et al., 2010). The performances of the 10 cross-validated network models were significantly better than chance for predicting the average SPP behavior: DMN-FPN (SMSE=0.87, $p<0.001$), FPN-FPN (SMSE=0.87, $p<0.001$), CON-DMN (SMSE=0.94, $p<0.001$), FPN-OccN (SMSE=0.94, $p<0.002$), FPN-SMN (SMSE=0.95, $p<0.01$), OccN-OccN (SMSE=0.97, $p<0.05$), DMN-DMN (SMSE=0.92, $p<0.05$), DMN-SMN (SMSE=0.95, $p<0.001$), SMN-SMN (SMSE=0.91, $p<0.001$), CON-SMN (SMSE=0.92, $p<0.001$) (**Figure 8**).

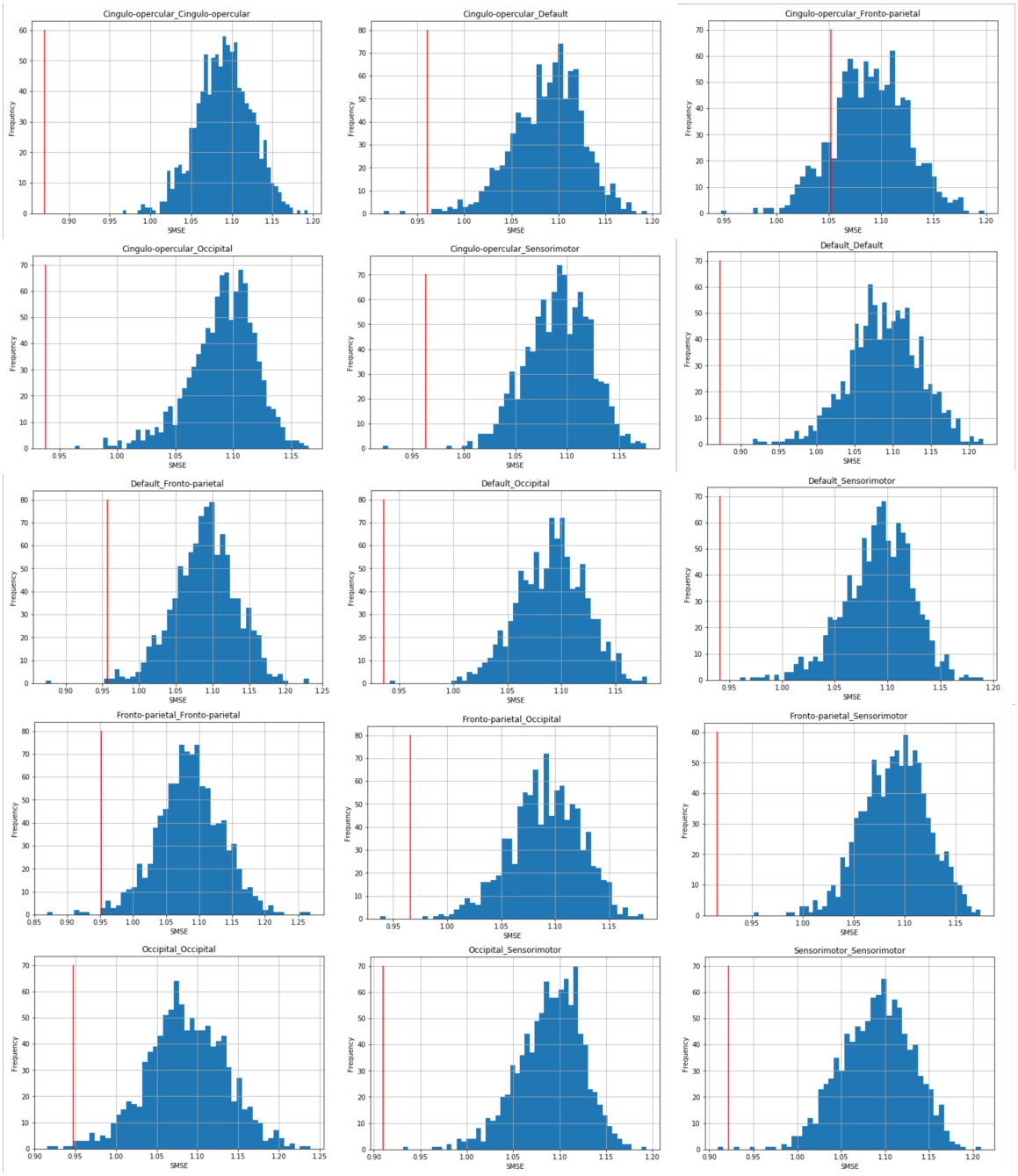

Figure 8. Results of Permutation Test for Second-Party Punishment Behavior.

The significance of performance (i.e., standard mean square error, SMSE, red dot line) are shown for the 15 cross-validated prediction models (five intra-networks and ten inter-networks) based on the permutation approach.

Ranking Network Procedure. After comparing the regression model performances, the 15*15 p-value matrix (i.e., distributions between the original and permutation-based prediction errors for each network) between the 15 networks (i.e., five intra-networks and ten inter-between networks) was computed (**Table 1**).

Table 1. P-Value Matrix for Ranking Performance of Models.
Numbers in this table are the p-value of the network pairs. The lower the p-value is, the better the network pair is.

Variables	1	2	3	4	5	6	7	8	9	10	11	12	13	14	15
DMN_FPN	0	0	0	0	0	0	0	0	0	0	0	0	0	0.042	0
CON_FPN	0.27	0	0.406	0.307	0	0	0	0.473	0.326	0	0.496	0.38	0.355	0.009	0
OccN_SMN	0.352	0	0	0.377	0	0	0	0	0.401	0	0	0.472	0.417	0.01	0
DMN_OccN	0.455	0	0	0	0	0	0	0	0	0	0	0	0	0.034	0
CON_OccN	0.159	0.367	0.271	0.16	0	0	0	0.319	0.208	0	0.354	0.252	0.236	0	0
FPN_FPN	0.213	0.356	0.287	0.2	0.478	0	0	0.337	0.234	0	0.362	0.288	0.265	0.012	0
CON_CON	0.05	0.118	0.08	0.047	0.169	0.238	0	0.093	0.05	0	0.121	0.07	0.089	0	0.276
CON_DMN	0.296	0	0.431	0.308	0	0	0	0	0.347	0	0	0.404	0.37	0.007	0
FPN_OccN	0.434	0	0	0.478	0	0	0	0	0	0	0	0	0	0.025	0
FPN_SMN	0.073	0.137	0.11	0.053	0.21	0.252	0.513	0.124	0.067	0	0.141	0.087	0.106	0.002	0.272
OccN_OccN	0.257	0	0.427	0.278	0	0	0	0.476	0.33	0	0	0.372	0.344	0.008	0
DMN_DMN	0.393	0	0	0.399	0	0	0	0	0.43	0	0	0	0.431	0.018	0
DMN_SMN	0.475	0	0	0.489	0	0	0	0	0.512	0	0	0	0	0.066	0
SMN_SMN	0	0	0	0	0	0	0	0	0	0	0	0	0	0	0
CON_SMN	0.148	0.298	0.244	0.151	0.418	0.462	0	0.277	0.163	0	0.297	0.215	0.196	0.004	0

CON, cingulo-opercular network; SMN, sensorimotor network; DMN, default mode network; FPN, frontoparietal network; OccN, occipital network.

The FPN-FPN network rank the highest in network ranking procedure, indicating that FPN (overlapping with CEN) predicted the average SPP behavior better than the other network pairs (**Figure 9**).

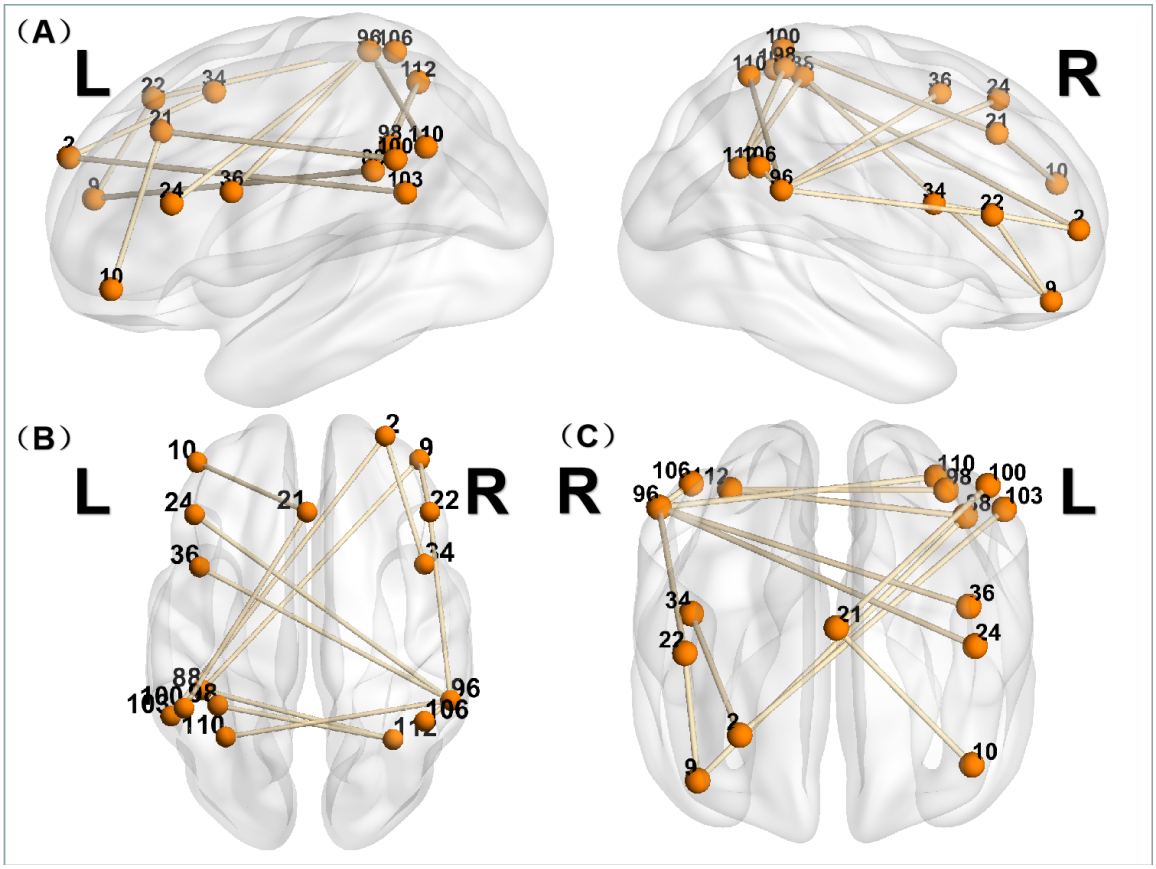

Figure 9. Resting -State Functional Connectivity Predicting Second-Party Punishment.

Resting-state functional connectivities (edges) between regions of interests (ROIs, nodes, shown in orange) of the frontoparietal network shown in sagittal view (A), axial view (B), and coronal view (C) predicted best the average second-party punishment behavior. The labels for ROIs (displayed as numbers) are given in Table S1 in Appendix.

4. DISCUSSION

Costly punishment, which means humans have the tendency to punish the violators of social norms at their own costs, plays a significant role in human life (Baumgartner, Götte, Gügler, & Fehr, 2012). In this study, we combined a SPP game with RS-fMRI and a prediction-analytics framework using MVPA to investigate whether individual differences in SPP can be predicted based on RSFC. At the behavioral level, the results showed that SPP increase with the degree of unfairness. SPP is higher than TPP. At the neuroimaging level, the findings demonstrated that individual variation of SPP behavior was predicted by RSFC in CEN (also known as FPN).

Our behavioral hypothesis was confirmed, showing that the more unfair the offer was, the higher was the SPP behavior. Previous research has shown that SPP is influenced by both intentions (of proposer) and outcome (for responder) (Gummerum & Chu, 2014; Krueger & Hoffman, 2016). SPP behavior was higher than for TPP behavior, because punishment is driven by blame, integrating intention of proposer and harm of receiver (F. X. Shen, Hoffman, Jones, & Greene, 2011). Second-parties blame more because they were more affected by the unfair offers; however, third-parties blame less since they were partial observer and not personally affected by those offers. Therefore, they rely their punishment decisions more on the intention of the proposer (Gummerum & Chu, 2014; Krueger & Hoffman, 2016).

Our neuroimaging hypothesis —the CEN is the most important network for predicting SPP behavior— was confirmed. SPP behavior engages three interacting large-

scale networks. The SAN— associated with *aversive self-related emotional experiences* that guide behavior— includes the dorsal anterior cingulate cortex (dACC) (detection of social norm violation), the anterior insula (AI) (generation of an aversive experience), and the amygdala (Amyg) (provides an emotional signal coding for the severity of harm, i.e., unfairness of the offer) (Bressler & Menon, 2010; Krueger & Hoffman, 2016).

The DMN —associated with social cognition, mentalizing, and theory of mind— is anchored in medial prefrontal cortex (mPFC) (Premack & Woodruff, 1978). This network integrated harm [via the ventromedial prefrontal cortex (vmPFC) connected to SAN] and the intent of the proposer [via the dorsomedial prefrontal cortex (dmPFC), including posterior cingulate cortex (PCC) for self-referential and temporo-parietal junction (TPJ) for intentions, beliefs or desires in others] into assessment of blame through the medial prefrontal cortex (mPFC) (P. Feng, Zheng, & Feng, 2016; Krueger & Hoffman, 2016).

The CEN —associated with higher-order cognition and decision making— converts the blame signal from the DMN into an actual decision, posterior parietal cortex (PPC) constructing a scale of punishment for dorsolateral prefrontal cortex (dlPFC) to select punishment that fits the norm violation (Bellucci et al., 2017; Bressler & Menon, 2010; Buckholtz et al., 2008, 2015; Krueger & Hoffman, 2016; Krueger, Hoffman, Walter, & Grafman, 2014).

Our findings confirm previous evidence that CEN —well understood in context-dependent assessments needed for higher-order cognition and decision making— plays a significant role in determining SPP behavior. In particular, when CEN converts the blame

signal into an actual punishment decision, it constructs a scale of punishment (PPC) and then selects a specific punishment within that scale (dlPFC) (Krueger & Hoffman, 2016).

The results of this study confirm a key role of PPC and dlPFC in SPP behavior. On the one hand, the PCC as part of the parietal cortex plays a key role in various cognitive functions, including attention, response selection, and quantitative numerical comparisons which may hint at a role for this area in constructing a punishment scale (Buckholtz et al., 2008). On the other hand, the dlPFC as part of the frontal cortex is involved in executive functions, i.e., an umbrella term for the management of cognitive processes such as working memory, cognitive flexibility, and planning). Hence, a key role of this region is to decide whether to punish or not based on an assessment of blame based on harm and intent. Previous research has shown that parietal and prefrontal activity is modulated by a punishment-related decision process, and especially activity in right dlPFC is higher when people decided to punish compared when not to punish (Buckholtz et al., 2008).

Although the novelty of our findings, several limitations exist in this study that need to be acknowledged. First, larger study samples are necessary for future studies to investigate SPP behavior based on RSFC, increasing the accuracy and lowering the error and variance of prediction. Additionally, costly punishment was measured in a single time point. Future studies should investigate SPP behavior in different time points to get a consistent result. Despite these limitations, this study extends the current knowledge about the underlying pinning of SPP behavior.

In summary, the study showed higher SPP behavior with increasing unfairness of offers. Further, the study indicated that average SPP behavior can be predicted through FC

among regions within CEN, the key network in determining the appropriate punishment behavior. The task-free fMRI approach in combination with a prediction-analytics framework confirms previous task-based fMRI findings— providing a comprehensive picture regarding SPP behavior.

In conclusion, this study helps to expand the knowledge about the underlying neural signatures of SPP behavior human to maintain the social norms and know the reason why humans are willing to punish the violators of social norms at their personal costs. Additionally, this study also provides a method to investigate people with brain disorder since it does not require objectives to understand the instruction.

APPENDIX

Table S1. Region of Interests Defined by Dosenbach's Atlas.
Characteristics (i.e., coordinates, hemisphere, label, and network) for each region of interest (ROI) of the Dosenbach' Atlas are shown.

	Coordinates						
Label	x	y	z	Hemisphere	Abbreviation	Region of Interest	Network
1	6	64	3	right	VMPFC	ventromedial prefrontal cortex	default mode netwotk
2	29	57	18	right	aPFC	anterior prefrontal cortex	fronto-parietal network
3	-29	57	10	left	aPFC	anterior prefrontal cortex	fronto-parietal network
4	0	51	32	-	mPFC	medial prefrontal cortex	default mode netwotk
5	-25	51	27	left	aPFC	anterior prefrontal cortex	default mode netwotk
6	9	51	16	right	VMPFC	ventromedial prefrontal cortex	default mode netwotk
7	-6	50	-1	left	VMPFC	ventromedial prefrontal cortex	default mode netwotk
8	27	49	26	right	aPFC	anterior prefrontal cortex	cingulo-opercular network
9	42	48	-3	right	vent-aPFC	ventral anterior prefrontal cortex	fronto-parietal network
10	-43	47	2	left	vent-PFC	ventral prefrontal cortex	fronto-parietal network
11	-11	45	17	left	VMPFC	ventromedial prefrontal cortex	default mode netwotk
12	39	42	16	right	VLPFC	ventral lateral prefrontal cortex	fronto-parietal network
13	8	42	-5	right	VMPFC	ventromedial prefrontal cortex	default mode netwotk
14	9	39	20	right	ACC	anterior cingulate cortex	default mode netwotk
15	46	39	-15	right	VLPFC	ventral lateral prefrontal cortex	default mode netwotk
16	40	36	29	right	DLPFC	dorsolateral prefrontal cortex	fronto-parietal network
17	23	33	47	right	sup-front	superior frontal gyrus	default mode netwotk
18	34	32	7	right	VPFC	ventral prefrontal cortex	cingulo-opercular network
19	-2	30	27	left	ACC	anterior cingulate cortex	cingulo-opercular network
20	-16	29	54	left	sup-front	superior frontal gyrus	default mode netwotk
21	-1	28	40	left	ACC	anterior cingulate cortex	fronto-parietal network
22	46	28	31	right	DLPFC	dorsolateral prefrontal cortex	fronto-parietal network
23	-52	28	17	left	VPFC	ventral prefrontal cortex	fronto-parietal network
24	-44	27	33	left	DLPFC	dorsolateral prefrontal cortex	fronto-parietal network
25	51	23	8	right	vFC	ventral frontal cortex	cingulo-opercular network

26	38	21	-1	right	AI	anterior insula	cingulo-opercular network
27	9	20	34	right	dACC	dorsal anterior cingulate cortex	cingulo-opercular network
28	-36	18	2	left	AI	anterior insula	cingulo-opercular network
29	40	17	40	right	dFC	dorsal prefrontal cortex	fronto-parietal network
30	-6	17	34	left	basal-ganglia	basal ganglia	cingulo-opercular network
31	0	15	45	-	mPFC	medial prefrontal cortex	cingulo-opercular network
32	58	11	14	right	frontal	frontal lobe	sensorimotor network
33	-46	10	14	left	vFC	ventral frontal cortex	cingulo-opercular network
34	44	8	34	right	dFC	dorsal prefrontal cortex	fronto-parietal network
35	60	8	34	right	dFC	dorsal prefrontal cortex	sensorimotor network
36	-42	7	36	left	dFC	dorsal prefrontal cortex	fronto-parietal network
37	-55	7	23	left	vFC	ventral frontal cortex	sensorimotor network
38	-20	6	7	left	basal-ganglia	basal ganglia	cingulo-opercular network
39	14	6	7	right	basal-ganglia	basal ganglia	cingulo-opercular network
40	-48	6	1	left	vFC	ventral frontal cortex	cingulo-opercular network
41	10	5	51	right	pre-SMA	pre-supplementary motor area	sensorimotor network
42	43	1	12	right	vFC	ventral frontal cortex	sensorimotor network
43	0	-1	52	-	SMA	supplementary motor area	sensorimotor network
44	37	-2	-3	right	mid-insula	middle insula	cingulo-opercular network
45	53	-3	32	right	frontal	frontal lobe	sensorimotor network
46	58	-3	17	right	PreCG	precentral gyrus	sensorimotor network
47	-12	-3	13	left	thalamus	thalamus	cingulo-opercular network
48	-42	-3	11	left	mid-insula	middle insula	sensorimotor network
49	-44	-6	49	left	PreCG	precentral gyrus	sensorimotor network
50	-26	-8	54	left	parietal	parietal lobe	sensorimotor network
51	46	-8	24	right	PreCG	precentral gyrus	sensorimotor network
52	-54	-9	23	left	PreCG	precentral gyrus	sensorimotor network
53	44	-11	38	right	PreCG	precentral gyrus	sensorimotor network
54	-47	-12	36	left	parietal	parietal lobe	sensorimotor network
55	33	-12	16	right	mid-insula	middle insula	sensorimotor network
56	-36	-12	15	left	mid-insula	middle insula	sensorimotor network
57	-12	-12	6	left	thalamus	thalamus	cingulo-opercular network
58	11	-12	6	right	thalamus	thalamus	cingulo-opercular network
59	32	-12	2	right	mid-insula	middle insula	cingulo-opercular network
60	59	-13	8	right	temporal	temporal lobe	sensorimotor network

61	-30	-14	1	left	mid-insula	middle insula	cingulo-opercular network
62	-38	-15	59	left	parietal	parietal lobe	sensorimotor network
63	52	-15	-13	right	IT	inferior temporal gyrus	default mode netwotk
64	-47	-18	50	left	parietal	parietal lobe	sensorimotor network
65	46	-20	45	right	parietal	parietal lobe	sensorimotor network
66	-55	-22	38	left	parietal	parietal lobe	sensorimotor network
67	-54	-22	22	left	PreCG	precentral gyrus	sensorimotor network
68	-54	-22	9	left	temporal	temporal lobe	sensorimotor network
69	41	-23	55	right	parietal	parietal lobe	sensorimotor network
70	42	-24	17	right	post-insula	posterior insula	sensorimotor network
71	11	-24	2	right	basal-ganglia	basal ganglia	cingulo-opercular network
72	-59	-25	-15	left	IT	inferior temporal gyrus	default mode netwotk
73	1	-26	31	right	PC	precuneus	default mode netwotk
74	18	-27	62	right	parietal	parietal lobe	sensorimotor network
75	-38	-27	60	left	parietal	parietal lobe	sensorimotor network
76	-30	-28	9	left	post-insula	posterior insula	cingulo-opercular network
77	-24	-30	64	left	parietal	parietal lobe	sensorimotor network
78	51	-30	5	right	temporal	temporal lobe	cingulo-opercular network
79	-41	-31	48	left	post-parietal	posterior parietal cortex	sensorimotor network
80	-4	-31	-4	left	PC	precuneus	cingulo-opercular network
81	54	-31	-18	right	fusiform	fusiform gyrus	cingulo-opercular network
82	-41	-37	16	left	temporal	temporal lobe	sensorimotor network
83	-53	-37	13	left	temporal	temporal lobe	sensorimotor network
84	28	-37	-15	right	fusiform	fusiform gyrus	default mode netwotk
85	-3	-38	45	left	PreC	precuneus cortex	default mode netwotk
86	34	-39	65	right	SPL	superior parietal lobule	sensorimotor network
87	8	-40	50	right	PreC	precuneus cortex	cingulo-opercular network
88	-41	-40	42	left	IPL	inferior parietal lobe	fronto-parietal network
89	58	-41	20	right	parietal	parietal lobe	cingulo-opercular network
90	-8	-41	3	left	PC	precuneus	default mode netwotk
91	-61	-41	-2	left	IT	inferior temporal gyrus	default mode netwotk
92	-28	-42	-11	left	Occ	occipital lobe	default mode netwotk
93	-5	-43	25	left	PC	precuneus	default mode netwotk
94	9	-43	25	right	PreC	precuneus cortex	default mode netwotk
95	43	-43	8	right	temporal	temporal lobe	cingulo-opercular network

96	54	-44	43	right	IPL	inferior parietal lobe	fronto-parietal network
97	-55	-44	30	left	parietal	parietal lobe	cingulo-opercular network
98	-35	-46	48	left	post-parietal	posterior parietal cortex	fronto-parietal network
99	42	-46	21	right	ST	superior temporal gyrus	cingulo-opercular network
100	-48	-47	49	left	IPL	inferior parietal lobe	fronto-parietal network
101	-41	-47	29	left	AG	angular gyrus	cingulo-opercular network
102	-59	-47	11	left	temporal	temporal lobe	cingulo-opercular network
103	-53	-50	39	left	IPL	inferior parietal lobe	fronto-parietal network
104	5	-50	33	right	PreC	precuneus cortex	default mode netwotk
105	-18	-50	1	left	Occ	occipital lobe	occipital network
106	44	-52	47	right	IPL	inferior parietal lobe	fronto-parietal network
107	-5	-52	17	left	PC	precuneus	default mode netwotk
108	10	-55	17	right	PC	precuneus	default mode netwotk
109	-6	-56	29	left	PreC	precuneus cortex	default mode netwotk
110	-32	-58	46	left	IPS	intra−parietal sulcus	fronto-parietal network
111	-11	-58	17	left	PC	precuneus	default mode netwotk
112	32	-59	41	right	IPS	intra−parietal sulcus	fronto-parietal network
113	51	-59	34	right	AG	angular gyrus	default mode netwotk
114	-34	-60	-5	left	Occ	occipital lobe	occipital network
115	36	-60	-8	right	Occ	occipital lobe	occipital network
116	46	-62	5	right	temporal	temporal lobe	occipital network
117	-48	-63	35	left	AG	angular gyrus	default mode netwotk
118	-52	-63	15	left	TPJ	temporoparietal junction	cingulo-opercular network
119	-44	-63	-7	left	Occ	occipital lobe	occipital network
120	19	-66	-1	right	Occ	occipital lobe	occipital network
121	11	-68	42	right	PreC	precuneus cortex	default mode netwotk
122	17	-68	20	right	Occ	occipital lobe	occipital network
123	-36	-69	40	left	IPS	intra−parietal sulcus	default mode netwotk
124	39	-71	13	right	Occ	occipital lobe	occipital network
125	-9	-72	41	left	Occ	occipital lobe	default mode netwotk
126	45	-72	29	right	Occ	occipital lobe	default mode netwotk
127	29	-73	29	right	Occ	occipital lobe	occipital network
128	-2	-75	32	left	Occ	occipital lobe	default mode netwotk
129	-29	-75	28	left	Occ	occipital lobe	occipital network
130	-16	-76	33	left	Occ	occipital lobe	occipital network

131	-42	-76	26	left	Occ	occipital lobe	default mode netwotk
132	9	-76	14	right	Occ	occipital lobe	occipital network
133	15	-77	32	right	Occ	occipital lobe	occipital network
134	20	-78	-2	right	Occ	occipital lobe	occipital network
135	-5	-80	9	left	postOcc	posterior occipital lobe	occipital network
136	29	-81	14	right	postOcc	posterior occipital lobe	occipital network
137	33	-81	-2	right	postOcc	posterior occipital lobe	occipital network
138	-37	-83	-2	left	postOcc	posterior occipital lobe	occipital network
139	-29	-88	8	left	postOcc	posterior occipital lobe	occipital network
140	13	-91	2	right	postOcc	posterior occipital lobe	occipital network
141	27	-91	2	right	postOcc	posterior occipital lobe	occipital network
142	-4	-94	12	left	postOcc	posterior occipital lobe	occipital network

REFERENCES

Arthurs, O., & Boniface, S. (2002). How well do we understand the neural origins of the fMRI BOLD signal? - ScienceDirect. *Trends in Neurosciences*, *25*(1), 27–31.

Beckmann, C. F., DeLuca, M., Devlin, J. T., & Smith, S. M. (2005). Investigations into resting-state connectivity using independent component analysis. *Philosophical Transactions of the Royal Society B: Biological Sciences*, *360*(1457), 1001–1013. https://doi.org/10.1098/rstb.2005.1634

Bellucci, G., Chernyak, S., Hoffman, M., Deshpande, G., Monte, O. D., Knutson, K. M., … Krueger, F. (2017). Effective connectivity of brain regions underlying third-party punishment: Functional MRI and Granger causality evidence. *Social Neuroscience*, *12*(2), 124–134. https://doi.org/10.1080/17470919.2016.1153518

Bellucci, G., Hahn, T., Deshpande, G., & Krueger, F. (2018). Functional connectivity of specific resting-state networks predicts trust and reciprocity in the trust game. *Cognitive, Affective, & Behavioral Neuroscience*. https://doi.org/10.3758/s13415-018-00654-3

Bellucci, G., Hahn, T., Deshpande, G., & Krueger, F. (2019). Functional connectivity of specific resting-state networks predicts trust and reciprocity in the trust game. *Cognitive, Affective, & Behavioral Neuroscience*, *19*(1), 165–176. https://doi.org/10.3758/s13415-018-00654-3

Biswal, B., Yetkin, F. Z., Haughton, V. M., & Hyde, J. S. (1995). Functional connectivity in the motor cortex of resting human brain using echo-planar mri. *Magnetic Resonance in Medicine*, *34*(4), 537–541. https://doi.org/10.1002/mrm.1910340409

Buckholtz, J. W., Asplund, C. L., Dux, P. E., Zald, D. H., Gore, J. C., Jones, O. D., & Marois, R. (2008). The Neural Correlates of Third-Party Punishment. *Neuron*, *60*(5), 930–940. https://doi.org/10.1016/j.neuron.2008.10.016

Buckholtz, J. W., & Marois, R. (2012). The roots of modern justice: cognitive and neural foundations of social norms and their enforcement. *Nature Neuroscience*, *15*, 655–661. https://doi.org/10.1038/nn.3087

Caspers, S., Schleicher, A., Bacha-Trams, M., Palomero-Gallagher, N., Amunts, K., & Zilles, K. (2013). Organization of the Human Inferior Parietal Lobule Based on Receptor Architectonics. *Cerebral Cortex*, *23*(3), 615–628. https://doi.org/10.1093/cercor/bhs048

Craddock, R. C., Holtzheimer, P. E., Hu, X. P., & Mayberg, H. S. (2009). Disease state prediction from resting state functional connectivity. *Magnetic Resonance in Medicine*, *62*(6), 1619–1628. https://doi.org/10.1002/mrm.22159

D'Amico Anthony V., Whittington Richard, Malkowicz S. Bruce, Schultz Delray, Schnall Mitch, Tomaszewski John E., & Wein Alan. (1995). A Multivariate Analysis of Clinical and Pathological Factors that Predict for Prostate Specific Antigen Failure after Radical Prostatectomy for Prostate Cancer. *Journal of Urology*, *154*(1), 131–138. https://doi.org/10.1016/S0022-5347(01)67248-3

Damoiseaux, J. S., Rombouts, S. a. R. B., Barkhof, F., Scheltens, P., Stam, C. J., Smith, S. M., & Beckmann, C. F. (2006). Consistent resting-state networks across healthy subjects. *Proceedings of the National Academy of Sciences*, *103*(37), 13848–13853. https://doi.org/10.1073/pnas.0601417103

de Blacam, C., Ogunleye, A. A., Momoh, A. O., Colakoglu, S., Tobias, A. M., Sharma, R., … Lee, B. T. (2012). High Body Mass Index and Smoking Predict Morbidity in Breast Cancer Surgery: A Multivariate Analysis of 26,988 Patients From the National Surgical Quality Improvement Program Database. *Annals of Surgery*, *255*(3), 551. https://doi.org/10.1097/SLA.0b013e318246c294

DE Gabrieli, J., Ghosh, S. S., & Whitfield-Gabrieli, S. (2015). Prediction as a Humanitarian and Pragmatic Contribution from Human Cognitive Neuroscience. *Neuron; Cambridge*, *85*(1), 11–26. http://dx.doi.org.mutex.gmu.edu/10.1016/j.neuron.2014.10.047

De Luca, M., Beckmann, C. F., De Stefano, N., Matthews, P. M., & Smith, S. M. (2006). fMRI resting state networks define distinct modes of long-distance interactions in the human brain. *NeuroImage*, *29*(4), 1359–1367. https://doi.org/10.1016/j.neuroimage.2005.08.035

Demers, M., Brodeur, J. M., Mouton, C., Simard, P. L., Trahan, L., & Veilleux, G. (1992). A multivariate model to predict caries increment in Montreal children aged 5 years. *Community Dental Health*, *9*(3), 273–281.

Dorsolateral prefrontal cortex. (2019). In *Wikipedia*. Retrieved from https://en.wikipedia.org/w/index.php?title=Dorsolateral_prefrontal_cortex&oldid=883673694

Dosenbach, N. U. F., Nardos, B., Cohen, A. L., Fair, D. A., Power, J. D., Church, J. A., … Schlaggar, B. L. (2010a). Prediction of individual brain maturity using fMRI. *Science (New York, N.Y.)*, *329*(5997), 1358–1361. https://doi.org/10.1126/science.1194144

Dosenbach, N. U. F., Nardos, B., Cohen, A. L., Fair, D. A., Power, J. D., Church, J. A., … Schlaggar, B. L. (2010b). Prediction of Individual Brain Maturity Using fMRI. *Science*, *329*(5997), 1358–1361. https://doi.org/10.1126/science.1194144

Feng, C., Deshpande, G., Liu, C., Gu, R., Luo, Y.-J., & Krueger, F. (2016). Diffusion of responsibility attenuates altruistic punishment: A functional magnetic resonance imaging effective connectivity study. *Human Brain Mapping*, *37*(2), 663–677. https://doi.org/10.1002/hbm.23057

Feng, P., Zheng, Y., & Feng, T. (2016). Resting-state functional connectivity between amygdala and the ventromedial prefrontal cortex following fear reminder predicts fear extinction. *Social Cognitive and Affective Neuroscience*, *11*(6), 991–1001. https://doi.org/10.1093/scan/nsw031

Finn, E. S., Shen, X., Scheinost, D., Rosenberg, M. D., Huang, J., Chun, M. M., … Constable, R. T. (2015). Functional connectome fingerprinting: identifying individuals using patterns of brain connectivity. *Nature Neuroscience*, *18*(11), 1664–1671. https://doi.org/10.1038/nn.4135

Gordon, E. M., Devaney, J. M., Bean, S., & Vaidya, C. J. (2015). Resting-State Striato-Frontal Functional Connectivity is Sensitive to DAT1 Genotype and Predicts Executive Function. *Cerebral Cortex (New York, NY)*, *25*(2), 336–345. https://doi.org/10.1093/cercor/bht229

Gospic, K., Mohlin, E., Fransson, P., Petrovic, P., Johannesson, M., & Ingvar, M. (2011). Limbic Justice—Amygdala Involvement in Immediate Rejection in the Ultimatum Game (Amygdala Involvement in the Ultimatum Game). *PLoS Biology*, *9*(5), e1001054. https://doi.org/10.1371/journal.pbio.1001054

Greicius, M. D., Flores, B. H., Menon, V., Glover, G. H., Solvason, H. B., Kenna, H., … Schatzberg, A. F. (2007). Resting-State Functional Connectivity in Major Depression: Abnormally Increased Contributions from Subgenual Cingulate Cortex and Thalamus. *Biological Psychiatry*, *62*(5), 429–437. https://doi.org/10.1016/j.biopsych.2006.09.020

Gummerum, M., & Chu, M. T. (2014). Outcomes and intentions in children's, adolescents', and adults' second- and third-party punishment behavior. *Cognition*, *133*(1), 97–103. https://doi.org/10.1016/j.cognition.2014.06.001

Hauert, C., Traulsen, A., Brandt, H., Nowak, M. A., & Sigmund, K. (2007). Via Freedom to Coercion: The Emergence of Costly Punishment. *Science*, *316*(5833), 1905–1907. https://doi.org/10.1126/science.1141588

Henrich, J., McElreath, R., Barr, A., Ensminger, J., Barrett, C., Bolyanatz, A., … Ziker, J. (2006). Costly Punishment Across Human Societies. *Science*, *312*(5781), 1767–1770. https://doi.org/10.1126/science.1127333

Heuvel, M. van den, Mandl, R., & Pol, H. H. (2008). Normalized Cut Group Clustering of Resting-State fMRI Data. *PLOS ONE*, *3*(4), e2001. https://doi.org/10.1371/journal.pone.0002001

Hillman, E. M. C. (2014). Coupling Mechanism and Significance of the BOLD Signal: A Status Report. *Annual Review of Neuroscience*, *37*, 161–181. https://doi.org/10.1146/annurev-neuro-071013-014111

Keller, C. J., Bickel, S., Honey, C. J., Groppe, D. M., Entz, L., Craddock, R. C., … Mehta, A. D. (2013). Neurophysiological investigation of spontaneous correlated and anticorrelated fluctuations of the BOLD signal. *The Journal of Neuroscience : The Official Journal of the Society for Neuroscience*, *33*(15), 6333. https://doi.org/10.1523/JNEUROSCI.4837-12.2013

Khadka, S., Meda, S. A., Stevens, M. C., Glahn, D. C., Calhoun, V. D., Sweeney, J. A., … Pearlson, G. D. (2013). Is Aberrant Functional Connectivity A Psychosis Endophenotype? A Resting State Functional Magnetic Resonance Imaging Study. *Biological Psychiatry*, *74*(6), 458–466. https://doi.org/10.1016/j.biopsych.2013.04.024

Krueger, F., & Hoffman, M. (2016). The Emerging Neuroscience of Third-Party Punishment. *Trends in Neurosciences*, *39*(8), 499–501. https://doi.org/10.1016/j.tins.2016.06.004

Kuwabara, K., & Yu, S. (2017). Costly Punishment Increases Prosocial Punishment by Designated Punishers: Power and Legitimacy in Public Goods Games. *Social*

Psychology Quarterly, *80*(2), 174–193. https://doi.org/10.1177/0190272517703750

Lee, M. H., Smyser, C. D., & Shimony, J. S. (2013). Resting state fMRI: A review of methods and clinical applications. *AJNR. American Journal of Neuroradiology*, *34*(10), 1866–1872. https://doi.org/10.3174/ajnr.A3263

Leibbrandt, A., & López-Pérez, R. (2012). An exploration of third and second party punishment in ten simple games. *Journal of Economic Behavior & Organization*, *84*(3), 753–766. https://doi.org/10.1016/j.jebo.2012.09.018

Logothetis, N. K., Pauls, J., Augath, M., Trinath, T., & Oeltermann, A. (2001). Neurophysiological investigation of the basis of the fMRI signal. *Nature*, *412*(6843), 150. https://doi.org/10.1038/35084005

McAuliffe, K. (20170406). Fairness overrides group bias in children's second-party punishment. https://doi.org/10.1037/xge0000244

Menon, V. (2011). Large-scale brain networks and psychopathology: a unifying triple network model. *Trends in Cognitive Sciences*, *15*(10), 483–506. https://doi.org/10.1016/j.tics.2011.08.003

Nash, K., Gianotti, L. R. R., & Knoch, D. (2015). A neural trait approach to exploring individual differences in social preferences. *Frontiers in Behavioral Neuroscience*, *8*. https://doi.org/10.3389/fnbeh.2014.00458

Oathes, D. J., Patenaude, B., Schatzberg, A. F., & Etkin, A. (2015). Neurobiological Signatures of Anxiety and Depression in Resting-State Functional Magnetic

Resonance Imaging. *Biological Psychiatry*, *77*(4), 385–393. https://doi.org/10.1016/j.biopsych.2014.08.006

Parisi, L., Rocca, M. A., Mattioli, F., Copetti, M., Capra, R., Valsasina, P., … Filippi, M. (2014). Changes of brain resting state functional connectivity predict the persistence of cognitive rehabilitation effects in patients with multiple sclerosis. *Multiple Sclerosis (Houndmills, Basingstoke, England)*, *20*(6), 686–694. https://doi.org/10.1177/1352458513505692

Radua, J., Phillips, M. L., Russell, T., Lawrence, N., Marshall, N., Kalidindi, S., … Surguladze, S. A. (2010). Neural response to specific components of fearful faces in healthy and schizophrenic adults. *NeuroImage*, *49*(1), 939–946. https://doi.org/10.1016/j.neuroimage.2009.08.030

Rockenbach, B., & Milinski, M. (2006). The efficient interaction of indirect reciprocity and costly punishment. *Nature*, *444*(7120), 718. https://doi.org/10.1038/nature05229

Salvador, R., Suckling, J., Coleman, M. R., Pickard, J. D., Menon, D., & Bullmore, E. (2005). Neurophysiological Architecture of Functional Magnetic Resonance Images of Human Brain. *Cerebral Cortex*, *15*(9), 1332–1342. https://doi.org/10.1093/cercor/bhi016

Sanchez, Z. M., Santos, M. G. R., Pereira, A. P. D., Nappo, S. A., Carlini, E. A., Carlini, C. M., & Martins, S. S. (2013). Childhood Alcohol Use May Predict Adolescent Binge Drinking: A Multivariate Analysis among Adolescents in Brazil. *The*

Journal of Pediatrics, *163*(2), 363–368. https://doi.org/10.1016/j.jpeds.2013.01.029

Shen, F. X., Hoffman, M. B., Jones, O. D., Greene, J. D., & Marois, R. (2011). Sorting Guilty Minds. *New York University Law Review; New York*, *86*(5), 1306.

Teipel, S. J., Born, C., Ewers, M., Bokde, A. L. W., Reiser, M. F., Möller, H.-J., & Hampel, H. (2007). Multivariate deformation-based analysis of brain atrophy to predict Alzheimer's disease in mild cognitive impairment. *NeuroImage*, *38*(1), 13–24. https://doi.org/10.1016/j.neuroimage.2007.07.008

van den Heuvel, M. P., & Hulshoff Pol, H. E. (2010). Exploring the brain network: A review on resting-state fMRI functional connectivity. *European Neuropsychopharmacology*, *20*(8), 519–534. https://doi.org/10.1016/j.euroneuro.2010.03.008

Voos, A., & Pelphrey, K. (2013). Functional Magnetic Resonance Imaging. *Journal of Cognition & Development*, *14*(1), 1–9. https://doi.org/10.1080/15248372.2013.747915

Wang, X., Han, Z., He, Y., Liu, L., & Bi, Y. (2012). Resting-State Functional Connectivity Patterns Predict Chinese Word Reading Competency. *PLoS ONE*, *7*(9). https://doi.org/10.1371/journal.pone.0044848

Wu, Y., Li, L., Yuan, B., & Tian, X. (2016). Individual differences in resting-state functional connectivity predict procrastination. *Personality and Individual Differences*, *95*, 62–67. https://doi.org/10.1016/j.paid.2016.02.016

BIOGRAPHY

Fengying Ding received a Bachelor of Engineering in 2015 after graduating from Beijing Institute of Technology, Zhuhai, China. Since 2017, she pursues her Master of Science in Bioinformatics and Computational Biology at George Mason University, VA, USA.